Journal of Advanced Research 49 (2023) 159–173

Contents lists available at ScienceDirect

Journal of Advanced Research

journal homepage: www.elsevier.com/locate/jare

Original Article

Paclitaxel-loaded ginsenoside Rg3 liposomes for drug-resistant cancer therapy by dual targeting of the tumor microenvironment and cancer cells

Ying Zhu [a,b], Anni Wang [a], Shuya Zhang [a], Jisu Kim [a], Jiaxuan Xia [a], Fengxue Zhang [d], Dan Wang [f], Qi Wang [d,e,*], Jianxin Wang [a,c,d,*]

[a] Department of Pharmaceutics, School of Pharmacy, Fudan University & Key Laboratory of Smart Drug Delivery, Ministry of Education, Shanghai 201203, China
[b] Department of Integrative Oncology, Fudan University Shanghai Cancer Center, Shanghai 200032, China
[c] Institute of Integrated Chinese and Western Medicine, Fudan University, Shanghai 200040, China
[d] Science and Technology Innovation Center, Guangzhou University of Chinese Medicine, Guangzhou 510405, China
[e] Institute of Clinical Pharmacology, Guangzhou University of Chinese Medicine, Guangzhou 510405, China
[f] Xiamen Ginposome Pharmaceutical Co., Ltd., Xiamen 361026, China

HIGHLIGHTS

- Functional Rg3-based liposomes loaded with paclitaxel (Rg3-PTX-LPs) can specifically distribute to MCF7/T cancer cells and TME simultaneously, mainly through the recognition of GLUT-1.
- Rg3-PTX-LPs can promote apoptosis of tumor cells and remodel TME to reverse the MDR state effectively.
- Rg3-PTX-LPs can repolarize protumor M2 macrophages to antitumor M1 phenotype, suppressing MDSCs, and decreasing TAFs and collagen fibers in TME by inhibiting the IL-6/STAT3/p-STAT3 pathway.

GRAPHICAL ABSTRACT

A schematic illustration of Rg3-PTX-LPs to reverse cancer drug resistance. (A) Ginsenoside Rg3 substitutes cholesterol as the membrane material in preparing Rg3-PTX-LPs. (B) The immunosuppressive and drug resistance tumor microenvironment. (C) Rg3-PTX-LPs downregulate the expression of Pgp and reduce the efflux of PTX from the cell. (D) Rg3-PTX-LPs remodel TME by inhibiting IL-6/STAT3/p-STAT3 pathway activation to repolarize protumor M2 macrophages to antitumor M1 phenotype, suppressing myeloid-derived suppressor cells (MDSCs), decreasing tumor-associated fibroblasts (TAFs) and collagen fibers in TME, and Inhibiting tumor angiogenesis.

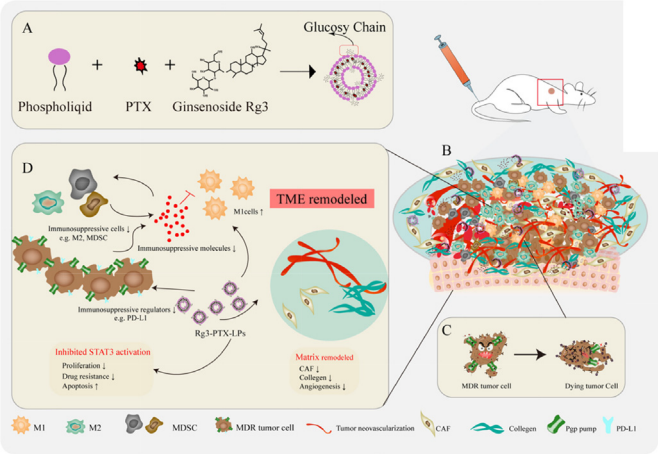

Peer review under responsibility of Cairo University.

* Corresponding authors at: Department of Pharmaceutics, School of Pharmacy, Fudan University & Key Laboratory of Smart Drug Delivery, Ministry of Education, Shanghai 201203, China; Institute of Clinical Pharmacology, Guangzhou University of Chinese Medicine, Guangzhou 510405, China.
E-mail addresses: wangqi@gzucm.edu.cn (Q. Wang), jxwang@fudan.edu.cn (J. Wang).

https://doi.org/10.1016/j.jare.2022.09.007
2090-1232/© 2022 The Authors. Published by Elsevier B.V. on behalf of Cairo University.
This is an open access article under the CC BY-NC-ND license (http://creativecommons.org/licenses/by-nc-nd/4.0/).

ARTICLE INFO

Article history:
Received 26 June 2022
Revised 16 September 2022
Accepted 19 September 2022
Available online 24 September 2022

Keywords:
MCF-7/T tumor
Ginsenoside Rg3
Paclitaxel
Liposomes
Multidrug resistance
Tumor microenvironment remodeling

ABSTRACT

Introduction: Inherent or acquired resistance to paclitaxel (PTX) is a pivotal challenge for chemotherapy treatment of multidrug-resistant (MDR) breast cancer. Although various targeted drug-delivery systems, including nanoparticles and liposomes, are effective for MDR cancer treatment, their efficacy is restricted by immunosuppressive tumor microenvironment (TME).
Methods: Ginsenosides Rg3 was used to formulate unique Rg3-based liposomes loaded with PTX to establish Rg3-PTX-LPs, which were prepared by the thin-film hydration method. The stability of the Rg3-PTX-LPs was evaluated by particle size analysis through dynamic light scattering. The active targeting effect of Rg3-based liposomes was examined in an MCF-7/T xenograft model by an in a vivo imaging system. To evaluate the antitumor activity and mechanism of Rg3-PTX-LP, MTT, apoptosis assays, TAM regulation, and TME remodeling were performed in MCF-7/T cells *in vitro* and *in vivo*.
Results: Rg3-PTX-LPs could specifically distribute to MCF7/T cancer cells and TME simultaneously, mainly through the recognition of GLUT-1. The drug resistance reversing capability and *in vivo* antitumor effect of Rg3-PTX-LPs were significantly improved compared with conventional cholesterol liposomes. The TME remodeling mechanisms of Rg3-PTX-LPs included inhibiting IL-6/STAT3/p-STAT3 pathway activation to repolarize protumor M2 macrophages to antitumor M1 phenotype, suppressing myeloid-derived suppressor cells (MDSCs), decreasing tumor-associated fibroblasts (TAFs) and collagen fibers in TME, and promoting apoptosis of tumor cells. Hence, through the dual effects of targeting tumor cells and TME remodeling, Rg3-PTX-LPs achieved a high tumor inhibition rate of 90.3%.
Conclusion: Our multifunctional Rg3-based liposome developed in the present study offered a promising strategy for rescuing the drug resistance tumor treatment.
© 2022 The Authors. Published by Elsevier B.V. on behalf of Cairo University. This is an open access article under the CC BY-NC-ND license (http://creativecommons.org/licenses/by-nc-nd/4.0/).

Introduction

Breast cancer is the most common malignancy in women, accounting for 25% of all cancers [1]. Surgery, radiation therapy, and chemotherapy are the primary treatments for breast cancer [2]. Multidrug resistance (MDR) severely hampers chemotherapy's effectiveness in treating breast cancer [3]. MDR involves several mechanisms, including (1) overexpression of drug efflux transporters like MDR protein (MRP) and P-glycoprotein (P-gp), which cause drug resistance when expressed in drug-sensitive tumor cells [4]. P-gp binds to varied small molecules, especially those with hydrophobic domains and positively charged regions, such as paclitaxel [5], therefore, it can undergo an ATP-dependent conformational change to move the substrate outside the cell (2) Programmed death-ligand PD-L1 is also closely related to chemotherapeutic drug resistance in tumors [6-9]. For instance, in HCC cells, transcriptional upregulation of PD-L1 results in MDR1 overexpression [5]. (3) In the tumor microenvironment (TME), tumor-associated fibroblasts (TAFs), tumor-associated macrophages (TAMs), and vascular endothelial cells can contribute to anticancer drug resistance. Fibroblasts represent a large population of the cells found in the TME, which can synthesize matrix components, such as collagen and fibrin, and play a structural role in matrix formation. TAFs are a subtype of activated fibroblasts in the TME that can promote tumorigenic potential and cell growth by reshaping the extracellular matrix [10]. As a significant participant in the TME, TAMs promote tumor progression, angiogenesis, and chemoresistance by polarizing from the M1 type to the M2 type [11]. M2 macrophage infiltration in tumors at high levels has a hand on drug resistance and can lead to the failure of chemotherapy. TAMs-derived IL-6 activates STAT3 to promote chemotherapy resistance, as has been demonstrated [12,13]. Vascular endothelial cells are also a key component of TME and can promote angiogenesis and tumor drug resistance [14]. Tumor cells benefit from the TME in general because it provides an environment in which they can survive and escape chemotherapy treatments, which diminishes tumor cell susceptibility to chemotherapeutic agents and leads to drug resistance.

Thus, an effective therapy against MDR tumors should target both cancer cells and the TME simultaneously. The combination of different drugs has been proved to be an effective approach [15,16]. However, the efficacy was restricted by the low distribution of combined drugs in the tumor, and the difference in drug levels at tumor sites caused by their *in vivo* pharmacokinetics [17]. Therefore, it is necessary to develop systems that can load various drugs and deliver them to the tumor *in vivo*. Nanotechnology-based carriers have been applied to encapsulate co-administrated drugs for tumor targeting combination therapy and yielded a relatively identical *in-vivo* fate for the drugs in the blood and tumor accumulation [18]. For example, polymeric nanoparticles, liposomes, dendrimers, and micelles. Among them, liposomes are well studied because of their biocompatibility, easy modification, and loading capability for hydrophilic and hydrophobic drugs. Liposomes encapsulating irinotecan/floxuridine showed promising results in phase II trials for colorectal cancer, while cytarabine/daunorubicin liposomes are currently in phase III clinical trials for acute myeloid leukemia after showing significantly lower toxicity and improved efficacy compared to the free drug combination [19].

Radix Ginseng's active ingredient, ginsenoside Rg3, can not only promote apoptosis in tumor cells [20,21], inhibit tumor invasion [22], proliferation [23], and angiogenesis [24], but also suppress metastasis and recurrence [25]. A recent study showed that Rg3 can reverse the MDR of some tumor types *in vitro* [26-28]. Seung et al. reported that Rg3 can reverse drug resistance mediated by P-gp [29]. Additionally, Rg3 can reduce PD-L1 expression induced by drug resistance, restore T-cell cytotoxicity, and inhibit A549/DDP cells proliferation and cisplatin resistance in cells [30]. Moreover, Rg3 has a TAM-regulatory function and regulates the differentiation of protumor M2 macrophages to the antitumor M1 phenotype when combined with chemotherapy [31]. Ginsenoside Rg3, the active ingredient in *ShenYi Capsule*, was approved as an anti-tumor drug in China in 2003. In clinical studies, a combination of *ShenYi Capsule* and various chemotherapeutics had a significant therapeutic effect on drug-resistant cancers [32-34]. Thus, Rg3 is a good option for MDR treatment in combination with chemotherapy drugs. Inspired by these findings, we hypothesized that co-delivery of ginsenoside

Rg3 and a chemotherapy drug in a liposomal carrier would significantly improve therapeutic efficacy on MDR cancer.

Often, tumor cells overexpress nutrient transporters to meet their increasing nutrient requirements for survival due to their metabolism and rapid proliferation. For cancer drug delivery, biomimetic nutrient transporter systems are being extensively investigated [35]. Various transporters, including glucose transporters, mannose receptors, low-density lipoprotein receptors, transferrin receptors, and albumin-binding proteins, may serve as drug delivery portal [36]. Particularly, GLUT-1 is highly expressed in malignant cells and endothelial cells of tumor-vessels associated with neoplasms [37-40], where it mediates the transport of glucose as well as other similar substances [36,41]. Rg3 has a hydrophobic domain with a steroid structure in character with that of cholesterol which is the indispensable main ingredient of liposomes and a hydrophilic domain with two glucosyl groups. Therefore, we inferred that Rg3 could not only be substitute for cholesterol as liposomal membrane material but also increase the uptake efficiency of liposomes by tumor cells through its recognition by GLUT-1. Indeed, we previously demonstrated that Rg3 could be a liposomal membrane material, whose glucosyl side chains can bind to the preferable amino acid residues of GLUT-1 [42,43]. In virtue of the physicochemical features and strong anti-tumor activities of ginsenoside Rg3, we have now established functional Rg3-based liposomes loaded with paclitaxel (PTX) to treat PTX-resistance breast cancer. We expected that the functional Rg3-based liposomes would effectively target and remodel the TME to reverse MDR state, effectively deliver PTX into tumors, and synergistically improve the therapeutic impact of PTX treatment (see Scheme 1).

Materials and Methods

Materials

Cholesterol was acquired from the Sinopharm Chemical Reagent Company (Shanghai, China).. Ginsenoside Rg3 was provided by Xiamen Bensu Pharmaceutical Technology (Xiamen, China). Coumarin-6 was purchased from Aladdin (Shanghai, China). Egg yolk phospholipid (EPC) was acquired from AVT Pharmaceutical Company (Shanghai, China). PTX was acquired from Dalian Meilun Biotechnology Company (Shanghai, China). Sigma-Aldrich provided the DAPI (St. Louis, MO, USA). Beijing Fanbo Science and Technology Company provided DiD and DiR. (Beijing, China). Most of the antibodies were procured from Novus Biologicals Company (Minneapolis, MN, USA), unless stated otherwise. ATCC (VA, USA) provided the MCF-7/T cell line, and the MCF-7 cells came from the Chinese Academy of Sciences' Shanghai Cell Bank (Shanghai, China). The Shanghai Laboratory Animal Center (SLAC) Co., Ltd. provided Balb/c nude mice (female, 3–5 w). All animal experiments were carried out according to protocols approved by Fudan University's ethical council (Shanghai, China).

Liposome preparation and characterization

As previously stated, ginsenoside Rg3 liposomes loaded with PTX (Rg3-PTX-LPs) and cholesterol liposomes loaded with PTX (C-PTX-LPs) were created. [42]. Briefly, thin-film hydration was used to prepare liposomes. EPC/Chol/PTX (20:6:3, w/w/w) for C-PTX-LPs and EPC/Rg3/PTX (20:6:3, w/w/w) for Rg3-PTX-LPs were the formulations per mL. The formulations of C-LPs and Rg3-LPs

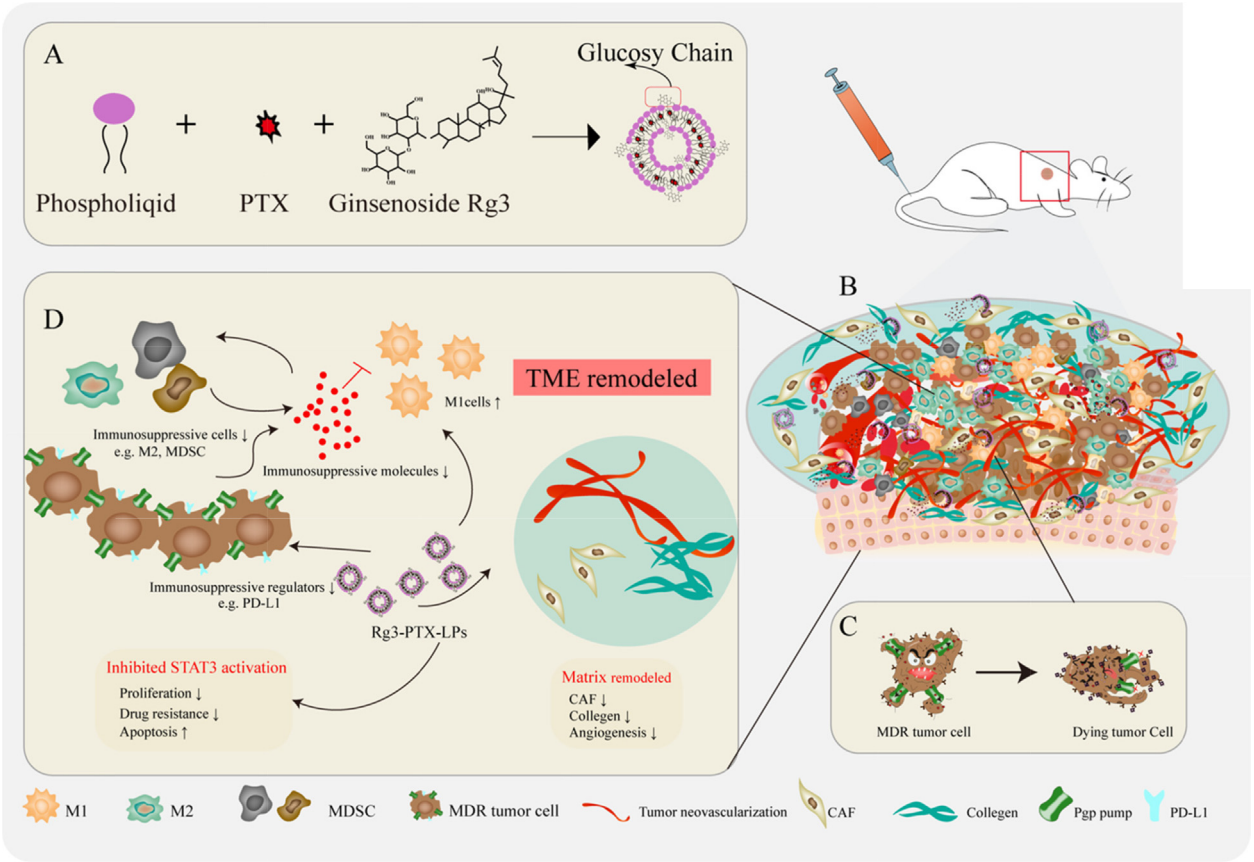

Scheme 1. A schematic illustration of Rg3-PTX-LPs to reverse cancer drug resistance. (A) Ginsenoside Rg3 substitutes cholesterol as the membrane material in preparing Rg3-PTX-LPs. (B) The immunosuppressive and drug resistance tumor microenvironment. (C) Rg3-PTX-LPs downregulate the expression of Pgp and reduce the efflux of PTX from the cell. (D) Rg3-PTX-LPs remodel TME by inhibiting IL-6/STAT3/p-STAT3 pathway activation to repolarize protumor M2 macrophages to antitumor M1 phenotype, suppressing myeloid-derived suppressor cells (MDSCs), decreasing tumor-associated fibroblasts (TAFs) and collagen fibers in TME, and Inhibiting tumor angiogenesis

are the same as previously mentioned but without PTX. The film components were dissolved in a 1:1 ethanol/chloroform solution. Liposomes labeled with fluorescence were created by adding the necessary amounts of coumarin-6/DiD/DiR to the lipid solutions before evaporation.

A zeta sizer nanoparticle analyzer (Malvern, UK) was used to determine the size and zeta potential of C-PTX-LPs and Rg3-PTX-LPs. Liposomes were detected using transmission electron microscopy (TEM) after being negatively stained with 2% phosphotungstic acid. High-performance liquid chromatography (HPLC; Agilent, USA) was used to determine the PTX encapsulation efficiency and drug-loading capacity [44], which were estimated using the following formulas:

$$\text{Encapsulation efficiency}(\%) = \frac{\text{encapsulated PTX (Weight)}}{\text{PTX added (Weight)}} \times 100\% \quad (1)$$

$$\text{Drug-loading capacity}(\%) = \frac{\text{encapsulated PTX (Weight)}}{\text{liposome material (Weight)}} \times 100\% \quad (2)$$

The liposomes' stability was assessed by measuring the turbidity of liposome dispersions for 72 h at 4 °C in phosphate-buffered saline (PBS, pH 7.4) or 37 °C in PBS containing 10% fetal bovine serum (FBS) The liposomes' average size and entrapment efficiency were assessed daily. *In vitro* drug release was assessed using dialysis [45] and a membrane with a molecular weight cut-off of 2.5 kDa in the release medium (PBS, consisting of 0.5% SDS and 10% FBS, pH 7.4,). Dialysis was carried out in a shaker at 37 °C. 500 μL medium was sampled and replenished with an equivalent amount of fresh release medium at predefined time intervals. HPLC was used to determine the drugs released.

Cell culture

Taxol-resistant MCF-7 human breast cancer cells (MCF-7/T) were cultured at 37 °C and 5% CO2 in RPMI-1640 medium (Gibco, USA) supplemented with 15% FBS, 500 ng/ml PTX, 100 U/mL penicillin, and 100 μg/mL streptomycin.

Cellular uptake assay in vitro

MCF-7/T cells were plated at 2×10^5 cells per well and cultured for 24 h. The plates were subsequently incubated with coumarin-6-labeled C-LPs and Rg3-LPs for an additional 4 h. The cells were then washed in cold PBS, resuspended in 200 μL PBS, and evaluated by flow cytometry. 5×10^4 cells were sown onto coverslips and cultivated for 24 h for qualitative examination. Then cells were rinsed and fixed with 4% paraformaldehyde for 25 min and stained with Hoechst 33,342 for 15 min after a 4-hour treatment with coumarin-6-labeled liposomes. The cells were then imaged by a confocal microscope. (LSM 710, Zeiss, Germany).

Evaluation of the cellular Rg3 liposome uptake mechanism

MCF-7/T cells were planted in 12-well plates at a density of 2×10^4 cells per well and cultivated for 24 h. The cells were subsequently given glucose or glucose receptor inhibitors, glucose (DG, 10 mM), phloridzin (2 mg/mL), and quercetin (2 mg/mL) for 60 min, with the control group receiving only DMEM. After incubation with the therapy, the cells were treated with coumarin-6-labeled Rg3-LPs and incubated for 4 h before the liposome suspension was withdrawn and the cells were rinsed with cold PBS. Subsequently, flow cytometry analysis was performed. Liposome uptake was calculated as a proportion of the fluorescence intensity of the control.

To validate that Rg3-LPs were transported by the GLUT-1 transporter, an *in-vitro* binding mechanism experiment was conducted. MCF-7/T cells were seeded at a density of 5×10^4 cells per well on coverslips and grown for 24 h. DiD-labeled Rg3-LPs were added to the cells and incubated at 4 °C for 4 h before being washed. The cells were then blocked for 60 min with 2% BSA in cold PBS before being treated overnight at 4 °C with a primary antibody against GLUT-1. After washing, the cells were treated with a Cy3-labeled secondary antibody and DAPI for 20 min at room temperature. Confocal microscopy revealed Rg3- LPs colocalization with GLUT-1 (LSM 710, Zeiss, Germany).

Evaluation of liposome penetration in MCF7/T tumor spheroids

After being prepared with a 2% (w/v) agarose gel, MCF-7/T cells were plated at 2×10^3 cells per well into a 96-well plate and cultivated for 7 days. The spheroids were treated with coumarin-6 tagged C-LPs or Rg3-LPs for 8 h. Then examine them by confocal microscopy after washing with PBS (LSM 710, Zeiss, Germany).

In-vitro cytotoxicity and apoptosis assays

A standard MTT test was used to determine the anticancer activity of the various medications. In a nutshell, cells were seeded at a density of 5×10^3 cells per well into 96-well plates and cultivated for 24 h. The cells were then cultured for 48 h with various doses of liposomes or free medicines. PTX concentrations in liposomes and free drugs were 0.08–20 μg/mL in MCF-7/T cells, while Rg3 concentrations were 0.16–40 μg/mL. PTX concentrations in liposomes and free drugs were 0.01–10 μg/mL in MCF-7 cells, while Rg3 concentrations were 0.02–20 μg/mL. The plates were subsequently incubated for additional 4 h after adding the MTT reagent (5 mg/mL, 20 μL). To test cell viability, each well was filled with 100 μL DMSO after the medium was removed, and the absorbance at 490 nm was measured with a microplate reader.

Apoptosis was analyzed by Annexin V-FITC/propidium iodide (PI) dual-labeling. MCF-7/T or MCF-7 cells were plated at a density of 1×10^5 cells per well and cultivated overnight. Then cells were given different liposomes or free drugs for 48 h. These experiments employed 20 μg/mL PTX and 40 μg/mL Rg3 for MCF-7/T cells. The cells were then collected and suspended in a 300 μL annexin V-FITC/PI apoptosis detection kit according to the manufacturer's instructions. Finally, the cells were examined by flow cytometry. (Cytomics FC 500).

MCF-7/T spheroid growth inhibition assay

After MC7-7/T spheroids were grown for 7 d and their diameter was approximately 400 μm. At a final concentrations of 20 μg/mL PTX and 40 μg/mL Rg3, the PTX alone, PTX/Rg3, C-PTX-LPs, and Rg3-PTX-LPs were given to the wells. MCF-7/T spheroids incubated in DMEM without PTX served as a control. At 0 h, 48 h, and 96 h after treatment, MCF-7/T spheroids were observed using an inverted microscope (DMI 4000B; Lecia, Germany).

Re-education of M2 macrophages in vitro

Mouse bone marrow-derived macrophages were collected and stimulated for M2 differentiation using standard procedures [46]. M2 macrophages were cultured in the top chambers of a Transwell cell culture plate, whereas MCF-7/T cells were cultured in the lower chambers. Then the alterations in the M2 phenotype after liposome administration were investigated. Liposomes equivalent to 20 μg/mL PTX and 40 μg/mL Rg3 or free drugs at the same con-

centrations were administered to the lower and upper chambers after a 12-hour co-culture, and the plates were incubated for another 48 h. TAMs were then collected and labeled with CD206 and CD86 antibodies. Flow cytometry was used to examine the cells (Cytomics FC 500).

In-vitro assay for measuring PD-L1 downregulation

MCF-7/T were planted at a density of 1×10^5 cells per well and grown overnight. The cells were subsequently given liposomes or free drugs, as mentioned previously. After that, cells were collected, rinsed, blocked, and incubated for 30 min with AF647-conjugated anti-PD-L1 antibody. Finally, flow cytometry was used to examine the cells (Cytomics FC 500). 5×10^4 cells were plated onto coverslips and grown for 24 h before being treated with Rg3 or Rg3-LPs at the indicated concentrations for 48 h. The cells were then blocked with 1% BSA in PBS and treated with AF 647-conjugated anti-PD-L1 for 30 min at 37 °C, followed by Hoechst staining. Confocal microscopy was used to look for PD-L1 expression (LSM 710, Zeiss, Germany).

An in-vivo imaging study of nude mice bearing MCF-7/T tumors

5×10^6 cells were implanted into the flanks of Balb/c nude mice to create a subcutaneous MCF-7/T tumor model. Tumor volume was calculated after about 2 weeks using the following formula:

$$V = \frac{L \times W^2}{2} \quad (3)$$

The mice were given DiD-loaded C-LPs or Rg3-LPs by tail vein injection when the tumor volume reached roughly 200 mm^3. At 1, 2, 4, 8, 12, and 24 h after administration with liposomes, the mice were photographed with an IVI Spectrum imaging equipment (PerkinElmer, USA), and subsequently sacrificed by cardiac perfusion. The heart, liver, spleen, lungs, kidneys, and tumors, were harvested. The IVI Spectrum equipment was used to image all of the organs. The tumors were fixed for 48 h before being dehydrated in 10% and 30% sucrose solutions and cryosectioned at a thickness of 10 μm (CM1950; Leica, Germany). Tumor tissue slices were treated with anti-GLUT-1 antibody overnight at 4°, then incubated with a Cy3-conjugated secondary antibody for 1 h, followed by DAPI dyeing for 15 min to determine colocalization of Rg3-LPs and GLUT-1. Confocal microscopy was used to analyze the tissue slices (LSM 710, Zeiss, Germany).

In-vivo anti-MCF-7/T efficacy assay

Subcutaneous MCF-7/T tumor-bearing nude mice were divided into five treatment groups when the tumor volume reached 200 mm3 (n = 5 in each group): the control group received saline, the PTX group, and the C-PTX-LPs group received 20 mg/kg PTX, and the PTX/Rg3 group and Rg3-PTX-LPs group received 20 mg/kg PTX + 40 mg/kg Rg3. Drugs, liposomes, and saline were injected into mouse tail veins every 3 d for 21 days. Throughout the experiment, body weight was recorded and tumor volume was determined using the formula above. The mice were euthanized at the end of the experiment, and the tumors and main organs were collected for histological analysis to determine the effects of each treatment group. A terminal deoxynucleotidyl transferase dUTP nick-end labeling (TUNEL) experiment was performed on the tumor tissues. Vessels and TAFs were characterized by using rabbit anti-mouse CD31 (GB12063, Servicebio, Shanghai, China) and rabbit-anti-mouse α-SMA (GB12063, Servicebio, Shanghai, China). Collagen fibers were stained with Masson's trichrome. All reagents were diluted as recommended by the manufacturer. A fluorescent microscope was used to capture the images (DMI 4000B; Leica, Germany). Using Fiji software, three randomly selected microscopic areas were quantitatively evaluated (Fiji Is Just ImageJ).

CD206 and iNOS antibodies were used to stain tumor slices to assess the expression of $CD206^+$ (M2 macrophages) and $iNOS^+$ cells (M1 macrophages), and PD-L1 in situ. Confocal microscopy was used to examine the tissue slices (LSM 710, Zeiss, Germany).

During the experimental endpoint, tumor tissues were dissected and the cells were collected by centrifugation at 2500 rpm for 5 min. The cells were then lysed with RIPA buffer (Beyotime, China). Anti-P-gp (ab80594, Abcam, UK), anti-PD-L1 (orb228661, Biorbyt, UK), anti-STAT 3 (ab76351, Abcam, UK), anti-p-STAT3 (phospho S727, ab76315, Abcam, UK), and anti-tubulin (Sigma-Aldrich, USA) antibodies were used to determine the levels of P-gp, PD-L1, STAT 3, and gel imaging analysis was used to assess band intensities after staining using a detection reagent (Millipore, USA) (ChemiDoc MPTM Imaging System; Bio-Rad, USA).

Flow-cytometry of TME immune cell populations

Flow cytometry was used to examine immune cell populations in tumor tissues obtained at the end of the study (BD Biosciences, USA). Extracellular labeling was performed on tumor cell suspensions, and cells were treated with antibodies against CD11b, Gr-1, CD45, F4/80, CD86, and CD206. BD Biosciences provided all antibodies, and flow-cytometric data was obtained using an LSRFortessa system (BD Biosciences). FlowJo software was used to examine the data (Tree Star).

Statistical analysis

GraphPad Prism 8 was used to analyze the data. T-tests or one-way ANOVA were used to compare data. Means were given as mean ± SD. We defined statistical significance as $p < 0.05$ and the symbols are explained in the figure legends.

Results and discussion

Liposomes preparation and characterization

DLS and TEM were used to examine the particle size distribution and morphology of liposomes. (Fig. 1A, B). C-PTX-LPs and Rg3-PTX-LPs had similar mean particle sizes of 127.9 ± 2.3 nm and 88.7 ± 0.99 nm, respectively, with a narrow particle size distribution and negative z-potential, and Rg3-PTX-LPs had superior encapsulation efficiency and drug loading capacity than C-PTX-LPs (Table S1, Supporting Information). The encapsulation efficiency and drug loading of Rg3 was 97.35% and 20.15%, respectively. TEM imaging showed that the liposomes were spherical and uniform in size. When incubated at 37 °C in PBS containing 10% FBS for 48 h, there were only minor changes in particle size, whereas particle size increased sharply at 72 h for both C-PTX-LPs and Rg3-PTX-LPs (Fig. 1C). This result indicates that the liposomes were expected to have good stability in circulating blood. Rg3-PTX-LPs showed a better sustained release effect than C-PTX-LPs, with an accumulative PTX release of<60% after 48 h, compared to nearly 80% for C-PTX-LPs (Fig. 1D). Furthermore, in our previous study, we determined that the release profile of Rg3 from Rg3-PTX-LPs at pH 5.5 and pH 6.4 were faster and more complete than that in pH 7.4 which might due to the rapid degradation and transformation of ginsenosides in acidic medium compared to neutral condition [43]. According to these findings, the functional Rg3-PTX-LPs were smaller in size, had better encapsulation and stability, and had a better sustained release effect than C-PTX-LPs. These

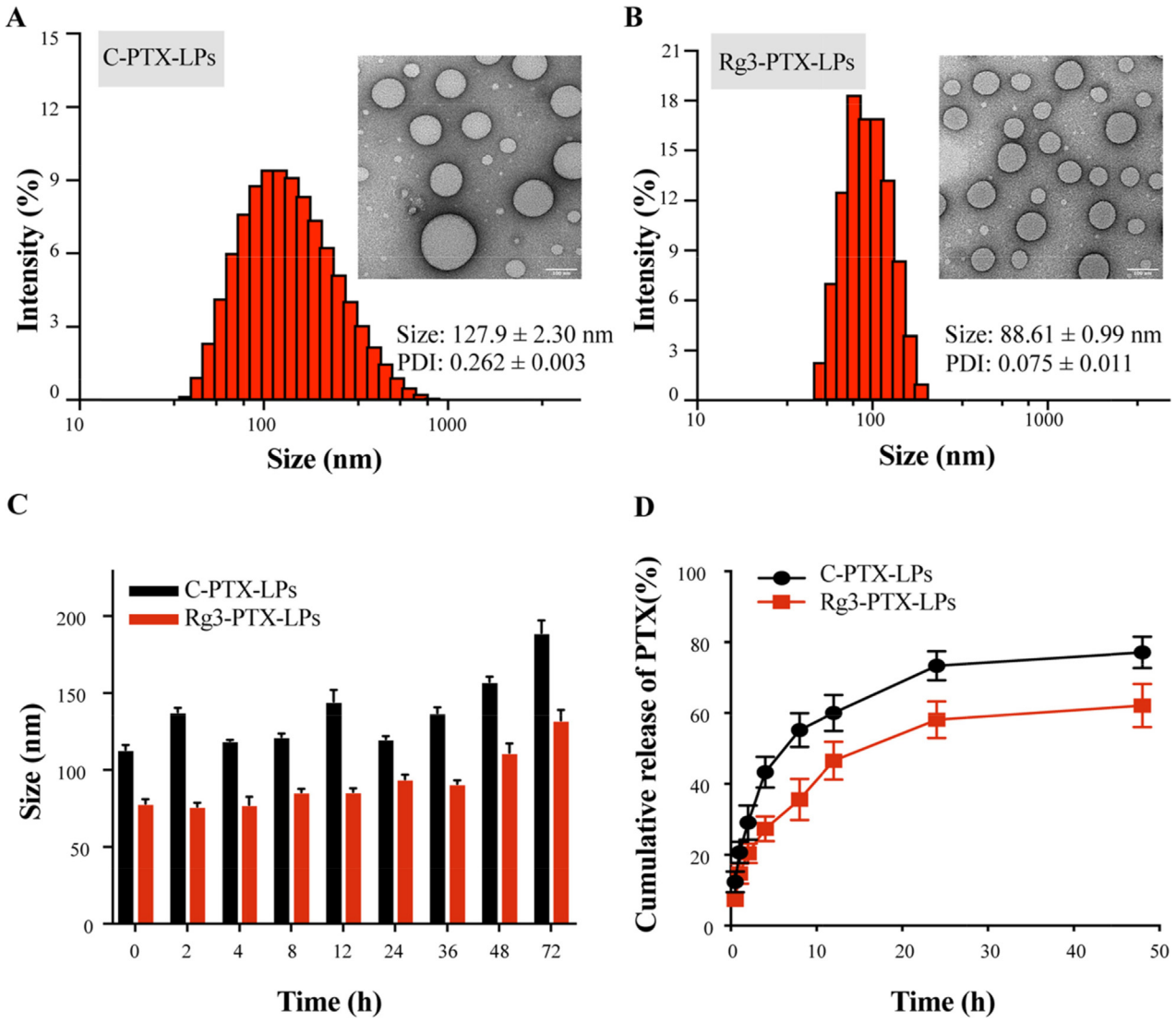

Fig. 1. Characterization of conventional cholesterol-based liposomes loaded with PTX (C-PTX-LPs) and ginsenoside Rg3-based liposomes loaded with PTX (Rg3-PTX-LPs). (A, B) Size distribution and morphology (inset) of C-PTX-LPs and Rg3-PTX-LPs as determined by dynamic light scattering (DLS) and TEM, respectively. (C) Liposome stability of the C-PTX-LPs and the Rg3-PTX-LPs was evaluated by measuring their size after incubation in PBS containing 10% FBS at 37 °C for 72 h. (D) PTX release profiles from C-PTX-LPs and Rg3-PTX-LPs, measured in PBS containing 10% FBS.

advantages of the Rg3-PTX-LPs may aid in the more effective targeting of tumor sites by drugs.

Cellular mechanism for Rg3 liposome uptake

Cellular uptake was evaluated using MCF-7/T cells and coumarin-6-labeled liposomes. Confocal microscopy and flow cytometry demonstrated that the fluorescence intensity in MCF-7/T cells treated with Rg3-LPs was considerably higher (~2 fold, $p < 0.001$) than in cells treated with C-LPs (Fig. 2A–C). This may have been due to the high expression of GLUT-1 on MCF-7/T cells and tumors [47]. GLUT-1 regulates the transport of molecules with similar structures to glucose, such as glucose analogs [48]. As the Rg3 structure contains two glucose molecules, the Rg3-LPs might be transported into tumor cells via GLUT-1. Rg3-LPs did bind to GLUT-1 *in vitro* (Fig. 2D), and flow cytometry demonstrated that Rg3-LPs uptake was significantly reduced in the presence of GLUT-1 inhibitors; There was reduction in the uptake efficiency of Rg3-LPs when the media contained excess glucose, indicating that glucose had competitive inhibition effect on transferring Rg3-LPs by GLUT-1 (Fig. 2E). For control, we performed a C-LPs inhibition experiment in MCF-7/T cells. As illustrated in Fig. S1, there is no significant difference in uptake efficiency between C-LPs and the other groups pretreated with glucose, phloridzin, and quercetin, indicating that these inhibitors have no effect on C-LPs uptake. These results imply that GLUT-1 is involved in the uptake of Rg3-LPs in MCF-7/T cells.

MCF-7/T tumor spheroid penetration of ginsenoside Rg3 liposomes

We inferred that Rg3-LPs were able to penetrate the tumor spheroids more efficiently than C-LPs due to the GLUT-1 transporter effect, resulting in higher liposome concentrations and better diffusion into the spheroids. To evaluate the penetration of Rg3-LPs, MCF-7/T cells were grown to develop spheroids. Interestingly, Rg3-LPs showed deeper tumor infiltration than C-LPs by multilayer confocal microscopy (Fig. 3A, B). The results revealed that Rg3, as the membrane material of the functional ginsenoside Rg3 liposomes, enhanced liposome uptake efficiency and penetration in spheroids.

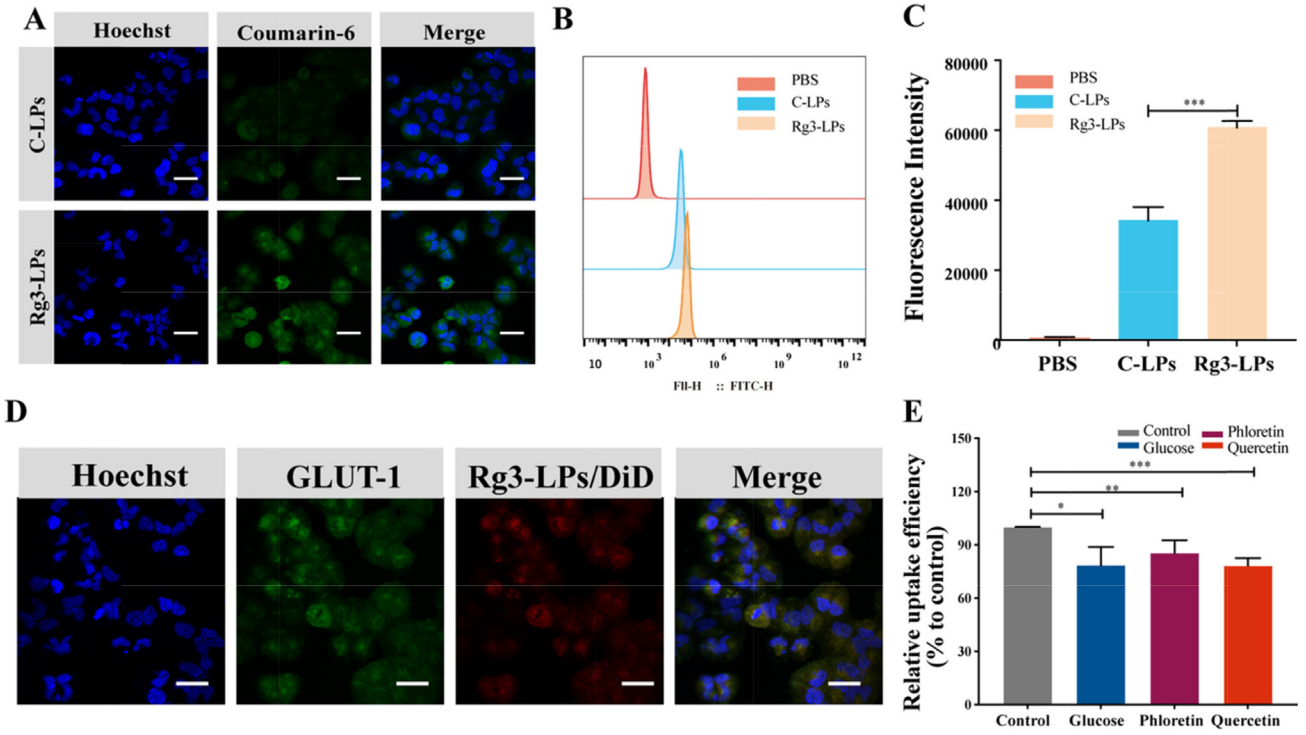

Fig. 2. Fluorescence analysis of the cellular uptake of courmarine-6-labeled C-LPs and Rg3-LPs in MCF-7/T cells. (A) Confocal fluorescence images of MCF-7/T cells in the presence of C-LPs or Rg3-LPs. (B) FACS analysis of cellular uptake of the liposomes. (C) Cellular uptake efficiency of C-LPs and Rg3-LPs. (D) *In vitro* binding of Rg3-LPs to MCF-7/T cells. Representative fluorescence images of Rg3-LPs and GLUT-1 localization in MCF-7/T cells. (E) Cellular uptake of Rg3-LPs in the presence of GLUT inhibitors relative to the control as determined by flow cytometry. Scale bar, 50 μm, Data are mean ± SD, n = 3. $^{*}p < 0.05$, $^{**}p < 0.01$, $^{***}p < 0.001$.

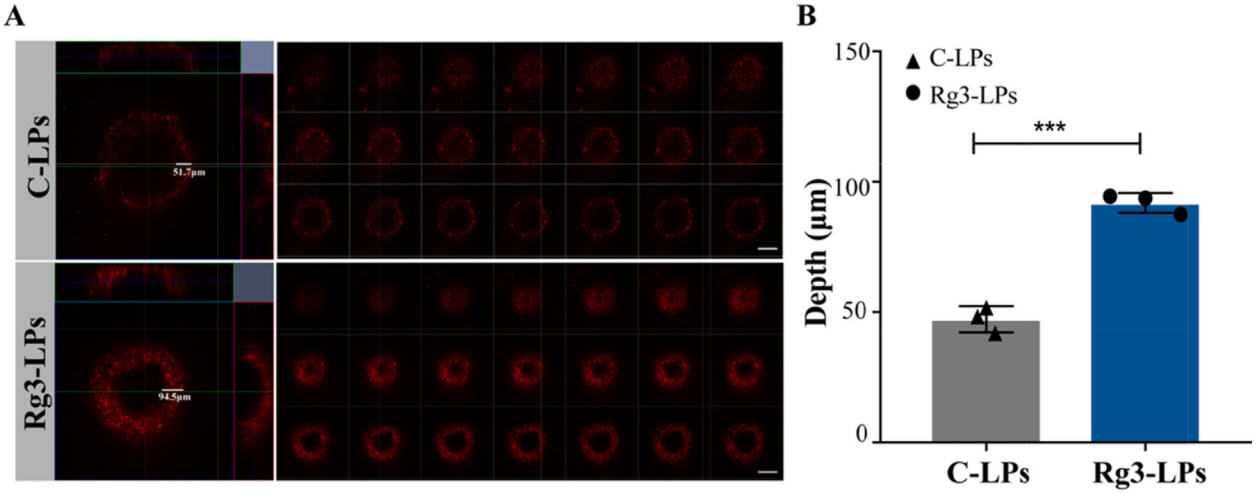

Fig. 3. Intra-tumoral accumulation of C-LPs and Rg3-LPs in 3D MCF-7/T cell tumor spheroids *in vitro*. (A) Fluorescence analysis with DiD by confocal microscopy. Fluorescence intensity is a function of the accumulation of C-LPs and Rg3-LPs. A higher fluorescence intensity was observed for Rg3-LPs than C-LPs. Scale bar, 200 μm. (B) Quantitative analysis of the penetration depth of C-LPs and Rg3-LPs in MCF-7/T spheroids. The panel shows confocal z-axis, continuous top-down scanning layers that are 5 mm for each depth level. Data are mean ± SD, n = 3, $^{*}p < 0.05$, $^{**}p < 0.01$, $^{***}p < 0.001$.

Anti-MDR cancer cell activity

As expected, MCF-7/T cell were not sensitive to PTX treatment alone, with a higher IC_{50} of approximately 13.02 μg/mL. While PTX/Rg3 combination therapy induced cytotoxicity in MCF-7/T cells, with an IC_{50} of approximately 6.24 μg/mL, while C-PTX-LPs had an IC_{50} of approximately 8.85 μg/mL. Interestingly, Rg3-PTX-LPs showed superior cytotoxicity compared to the other treatment groups, with an IC_{50} of 2.45 μg/mL (Fig. 4A, Table S2). The Rg3-PTX-LPs also had significant antitumor activity in normal MCF-7 cells with a much lower IC_{50} of 0.02 μg/mL (Fig. 4B; Table S3).

Flow cytometry was utilized to differentiate between cells in early apoptosis and late apoptosis [49]. For the PTX, PTX/Rg3, C-PTX-LPs, and Rg3-PTX-LPs groups, the proportion of apoptotic (early and late) cells was 11.95%, 30.20%, 28.65%, and 51.73%, respectively (Fig. 4C, D, Table S4). These findings showed that a

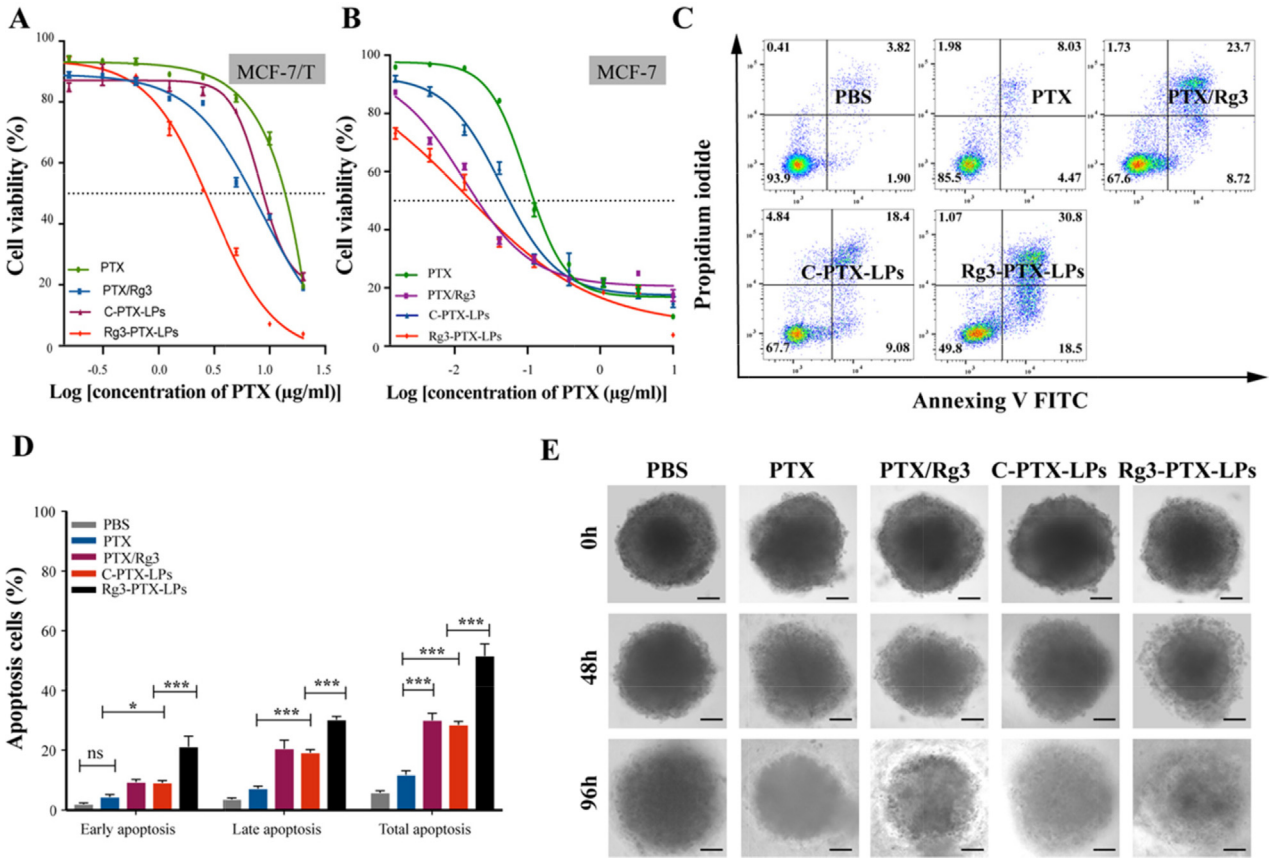

Fig. 4. *In vitro* anticancer activities of Rg3-PTX-LPs. (A) Cytotoxicity of different PTX formulations in MCF-7/T cells by MTT assay (n = 6). (B) Cytotoxicity of different PTX formulations in MCF-7 cells by MTT assay (n = 6). (C, D) Representative scatter plots of Annexin V/PI analysis of MCF-7/T cells treated with the various PTX formulations. The highest level of total apoptosis was observed for Rg3-PTX-LPs. (E) Representative microscopic images of MCF-7/T tumor spheroids after treatment with the different PTX formulations at 0 h, 48 h, 96 h. Scale bar, 100 μm. Data are mean ± SD, n = 3, $^{*}p < 0.05$, $^{**}p < 0.01$, $^{***}p < 0.001$.

combination of PTX and Rg3 could efficiently cause apoptosis in drug-resistant breast cancer cells, but that Rg3-PTX-LPs had a superior anticancer effect.

When the diameter of MCF-7/T tumor spheroids reached approximately 400 μm, various PTX formulations (PTX alone, PTX combine Rg3, C-PTX-LPs, Rg3-PTX-LPs) with a final PTX concentration of 20 μg/ml were applied to tumors to assess their growth-inhibitory effects. Tumor growth continued in the control group that did not receive drug treatment, while growth was suppressed in the treatment groups (Fig. 4E). MCF-7/T spheroids in the control group were concentrated while spheroids appeared slackened in the four drug treatment groups and their surfaces were disorganized to various degrees, with numerous necrotic cells appearing on the periphery, especially in the Rg3-PTX-LPs group. The stronger tumor-inhibitory impact reported in the Rg3-PTX-LPs therapy group could be due to better penetration and active cellular uptake. These findings indicated that PTX was delivered deeper into the tumor spheroid by Rg3-based liposome and exerted a synergistic antitumor effect with Rg3.

Mechanisms of the Rg3-PTX-LPs combination treatment

We next investigated the mechanisms of the combination treatment. P-gp is a cell-membrane protein that transports a variety of foreign chemicals out of cells. Our findings reveal that when Rg3 is present (as in the Rg3/PTX and Rg3-PTX-LPs groups), P-gp protein expression was downregulated in MCF-7/T cells (Fig. 5A, Figure S2). Indeed, it has been established that Rg3 can inhibit P-gp expression and reverse MDR [50]. PD-L1 was also downregulated in Rg3/PTX groups and this effect was enhanced with Rg3-PTX-LPs (Fig. 5B, C and Figure S3).

The TME plays a significant role in tumor progression regulation. Treatment outcomes are also influenced by drug effects on TME-associated cells, the bulk of which are TAMs. As a result, we looked into the impact of Rg3-PTX-LPs on TAMs. IL-4 and IL-10 stimulated macrophages to take on an active or M2 phenotype. [51], and ginsenoside Rg3 reportedly re-educates M2 cells to the M1 phenotype [31]. FACS analysis demonstrated that PTX/Rg3 and especially Rg3-PTX-LPs reduced CD206 expression and increased CD86 expression in MCF-7/T cells (Fig. 5D, E), suggesting that M2 macrophages are declining, while M1 macrophages are increasing. Both PTX and C-PTX-LPs decreased the population of M2 macrophages, but this effect was augmented in the presence of Rg3. These findings support observations that PTX mimics lipopolysaccharide activity in primary macrophages and macrophages. [52] and Rg3 can promote IFN-γ expression [53], which exerts a synergistic effect in the stimulation of the M1 phenotype.

In-vivo imaging analysis of ginsenoside Rg3 liposomes

We then measured the tumor-targeting effectiveness of Rg3-based liposomes loaded with DiD *in vivo*. Fluorescence was detected at the tumor within 1 h after injecting the Rg3-LPs loaded with DiD and gradually increased until 8 h after treatment (Fig. 6A, C), and the Rg3-LPs exhibited significantly higher tumor accumulation than C-LPs. *Ex vivo* imaging of dissected tissues revealed a higher tumor accumulation of Rg3-LPs than C-LPs (Fig. 6B, D and S4), suggesting an enhanced tumor delivery efficacy mediated by

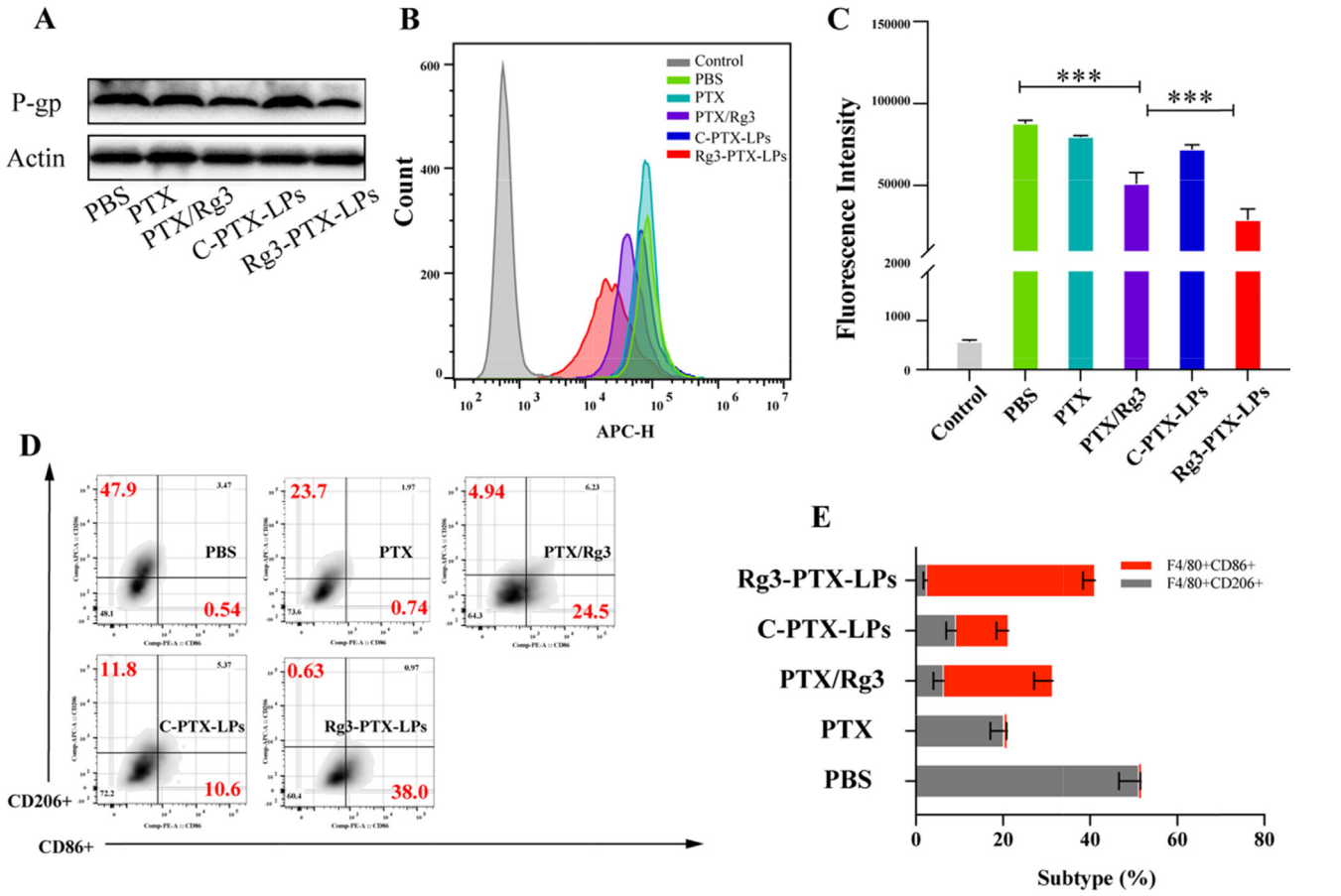

Fig. 5. *In vitro* P-gp and PD-L1 downregulation, and M2 phenotype macrophage re-education after different treatment. (A) P-gp expression in MCF-7/T cells. (B, C) FACS analysis of PD-L1 expression in MCF-7/T cells. (D, E) FACS analysis of CD206 and CD86 expression in M2 cells. Data are mean ± SD, n = 3, $^{*}p < 0.05$, $^{**}p < 0.01$, $^{***}p < 0.001$.

GLUT-1. Furthermore, we found that more Rg3-LPs accumulated in the liver than C-LPs, which might due to the smaller particle size of Rg3-LPs. Intra-tumoral infiltration assay results showed that both liposomes were distributed in tumor tissues, with stronger fluorescence intensity in the Rg3-LPs group (Fig. 6B), implying that they have the ability to penetrate the tumor barrier and allow for intra-tumoral penetration. This result was consistent with our previous *in vitro* spheroid penetration results. Notably, GLUT-1 colocalized with the Rg3-LPs (Fig. 6E), indicating that GLUT-1-mediated delivery appears to be a critical mechanism for their tumor targeting.

In-vivo therapeutic efficacy and mechanisms of Rg3-PTX-LPs in drug-resistant MCF-7/T breast cancer

An *in vivo* pharmacodynamics evaluation of Rg3-PTX-LPs was conducted in PTX-resistant breast tumor-bearing nude mice. PTX alone showed a slight tumor-suppressive effect when compared with PBS based on measurements of tumor growth and endpoint weight and size (Fig. 7A, B, C). Treatment with PTX/Rg3 and Rg3-PTX-LPs at dosages of 20 mg/kg PTX and 40 mg/kg Rg3, which resulted in considerable tumor shrinkage, with inhibition rates of 72.6% and 90.3%, respectively. However, C-PTX-LPs (20 mg/kg) and free PTX (20 mg/kg) induced inhibition rates of 64.9% and 34.1%, respectively (Table S5). Clearly, Rg3-PTX-LPs demonstrated the best antitumor activity among all treatments. The free-drug combination of 20 mg/kg PTX + 40 mg/kg Rg3 showed a higher efficacy than free 20 mg/kg PTX alone, suggesting a synergistic antitumor effect.

Expression of P-gp and PD-L1 are major MDR mechanisms. Western blotting revealed lower levels of P-gp and PD-L1 in the PTX/Rg3 and Rg3-PTX-LPs groups than in the other treatment groups (Fig. 7D, Figure S5). Immunofluorescence images confirmed that Rg3, especially in the form of Rg3-PTX-LPs, downregulated the expression PD-L1 in MCF-7/T xenografted tumors (Fig. 7F). These results were in accordance with our findings *in vitro*. The significant tumor growth-suppressive effect of Rg3-PTX-LPs was supported by TUNEL apoptosis assay results, which indicated the highest level of apoptosis in the Rg3-PTX-LPs group when compared to the other treatments (Fig. 7E).

TAFs, TAMs, and angiogenesis in the TME all play important roles in MDR development. TAFs in tumors not only secrete collagen and create an immunosuppressive microenvironment to support tumor-cell survival, but also secrete matrix-degrading enzymes such as metalloproteinases, and various compounds that induce drug resistance [54-57]. Therefore, the distribution of TAFs, collagen, and vessels in the tumor was determined by immunohistochemistry. The anti-CD31 staining revealed that there were fewer vessels in tumors in the Rg3-PTX-LPs group than in other groups (Fig. 8A). The combination therapy of both PTX/Rg3 and Rg3-PTX-LPs exhibited synergistic anti-angiogenesis, indicating that angiogenesis inhibition was the mechanism underlying this antitumor activity of the combination therapy. Labeling of the TAFs with α-SMA showed that the tumor stroma in the PBS control group had a massive fibrous structure; PTX/Rg3 and C-PTX-LPs attenuated the α-SMA-positive cells, whereas Rg3-PTX-LPs eliminated the fibroblasts almost entirely from the tumor tissue (Fig. 8B). These results indicate that the effect of combination ther-

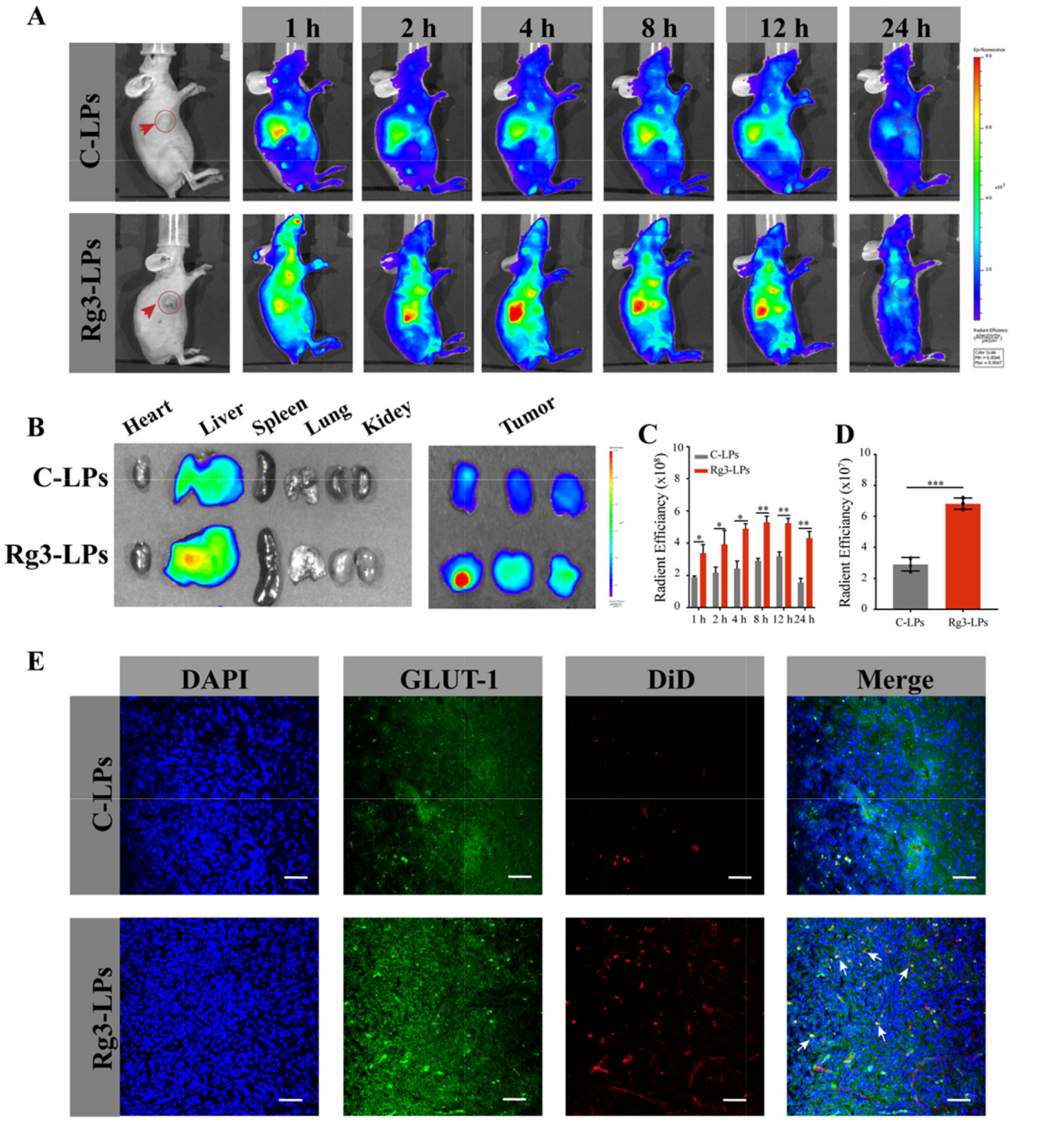

Fig. 6. *In vivo* distribution and tumor targeting of liposomes in a breast tumor mouse model. (A) *In vivo* fluorescence imaging of MCF-7/T subcutaneous xenograft tumor-bearing nude mice treated with DiR-loaded liposomes at the indicated time points. (B) *In vivo* radiant efficiency in main organs and tumors dissected from the nude mice. (C) Fluorescence imaging of dissected major organs and tumors. (D) *Ex vivo* radiant efficiency at the tumors. (E) Confocal images of the liposome distribution and colocalization of liposomes with GLUT-1 in tumor sections of MCF-7/T xenograft-bearing mice after systemic administration of DiD-loaded liposomes. Red: DiD, blue: nuclei, green: GLUT-1 antibody. Bar: 50 μm. Data are mean ± SD, n = 3, $^{*}p < 0.05$, $^{**}p < 0.01$, $^{***}p < 0.001$.

apy was enhanced by the Rg3-based liposomes. Collagen content was studied using Masson's trichrome stain [58] in the tumors after these treatments and indicated that PTX/Rg3 and Rg3-PTX-LPs decreased collagen expression and disrupted the collagen structure in tumors compared to the other treatments, with Rg3-PTX-LPs showing the best effect of all the groups (Fig. 8C).

The immune state in the TME at the treatment endpoint was analyzed by flow cytometry. M2 macrophages with anti-inflammatory properties overexpress CD206 and M1 macrophages with pro-inflammatory properties overexpress CD86 [59,60]. Thus, we measured M2 and M1 macrophage populations based on these markers. M2 and M1 macrophage frequencies were approximately 32% and 6.8%, respectively, in the PTX group, and 18% and 10.4% in the C-PTX-LPs group. Compared with the PBS group, M2 macrophages significantly decreased by approximately 13%, while M1 cells increased approximately 10.3% after treatment with the free-drug combination (Fig. 8D). Rg3-PTX-LPs exhibited the greatest ability to reduce the M2 population (∼4%) while increasing the

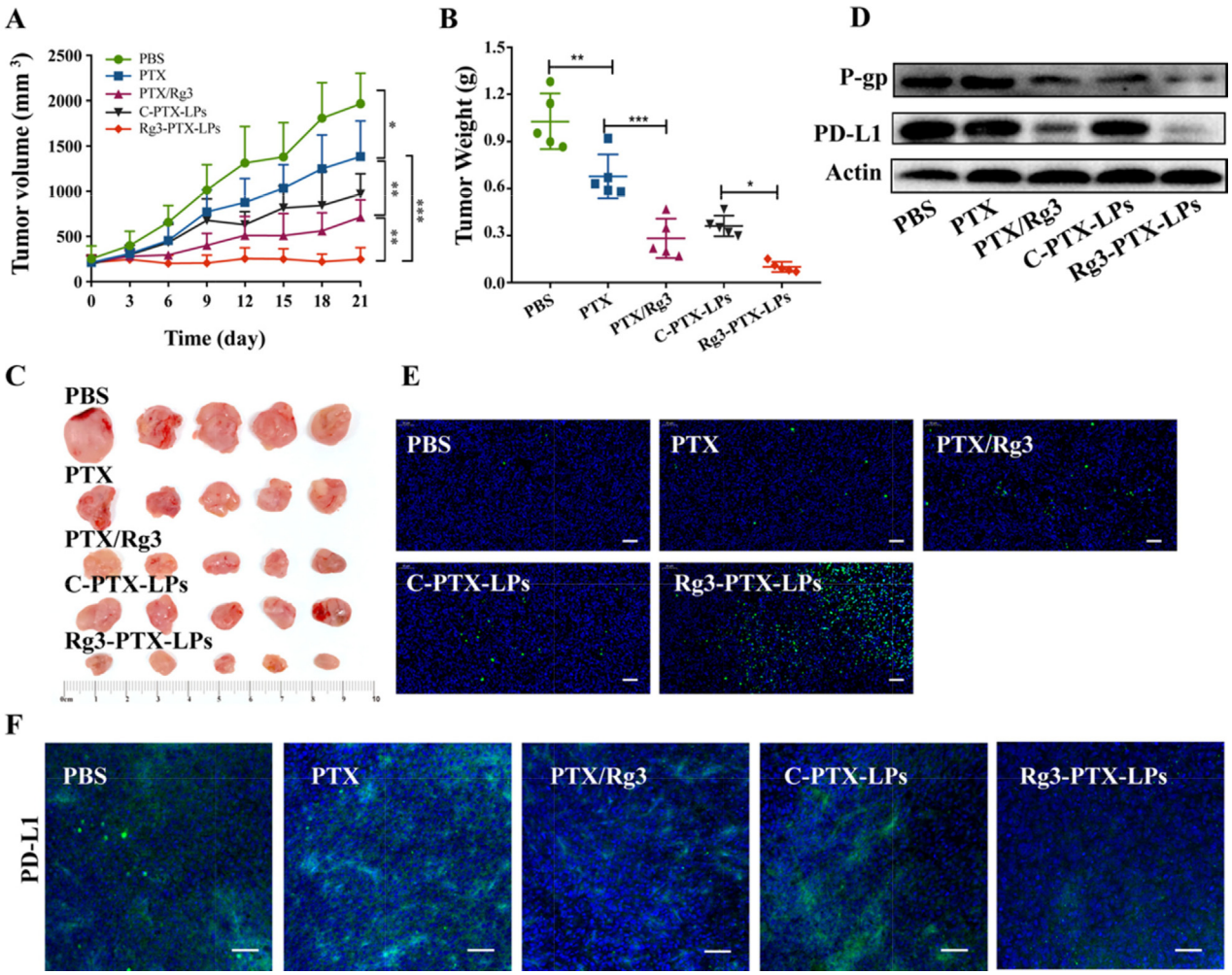

Fig. 7. Treatment efficacies in nude mice bearing MCF-7/T subcutaneous xenograft tumors. (A) Tumor growth curves. (B) Tumor weights. (C) Tumor sizes. (D) Western blotting of P-gp and PD-L1 expression in tumor tissues. (E) TUNEL assay of apoptosis in subcutaneous MCF-7/T tumors. Magnification, 10×, scale bar, 100 μm. (F) Expression of PD-L1 in MCF-7/T tumors tissues, scale bar, 50 μm. Data are mean ± SD, n = 6, $^{*}p < 0.05$, $^{**}p < 0.01$, $^{***}p < 0.001$.

M1 population (~29%), which was supported by the immunofluorescence staining results (Fig. 8F, H). Myeloid-derived suppressor cells (MDSCs) suppress the immune system. [61]. We found that the population of granulocytic (G-)MDSCs significantly decreased in tumors treated with PTX/Rg3, C-PTX-LPs, or Rg3-PTX-LPs, whereas tumors treated with PTX did not differ significantly from the control group (Fig. 8E). The population of monocytic (M-) MDSCs was strongly reduced only in the Rg3-PTX-LPs treatment group. These findings were consistent with the tumor volume and weight results reported in the treatment groups and indicated that the combination of Rg3 and PTX can considerably modulate the TME and increase its anti-tumor effect.

Constitutive activation of signal transducers and activators of transcription 3 (STAT3) can lead to immunosuppression [62]. Furthermore, STAT3 activation involved the up-regulation of P-gp[66] and treatment resistance, inhibiting STAT3 restores the efficacy of chemotherapeutic drugs [63]. In our study, western blotting revealed that the free-drug combination more strongly inhibited STAT3 activation (p-STAT3) and downregulation of P-gp than PTX or C-PTX-LPs treatments, while the effect of Rg3-PTX-LPs was the strongest. (Fig. 7D, 8I, Figure S6). When STAT3 is activated, TAMs that with p-STAT3 activation no longer exhibit antitumor effects in the TME, and they promote cancer cell progression in concert with MDSCs [64]. There may be crosstalk between STAT3 and the TME through signaling molecules such as IL-6, which can activate the STAT3 pathway as well as promote immune suppression [65]. ELISA results showed that in the Rg3/PTX and Rg3-PTX-LPs groups, IL-6 expression was significantly reduced compared to the other groups (Fig. 8J). Together, these results revealed at least some of the mechanisms underlying the PTX/Rg3 combination treatment and demonstrated that the therapeutic efficacy was strongly enhanced by a liposome formulation treatment strategy.

The biosafety of the treatments was evaluated by histological examination. There were no evident pathological alterations observed in any of the treatment groups (Fig. 9), and body weight did not significantly differ among the groups (Figure S7). These findings suggest that the multifunctional ginsenoside Rg3 liposome delivery system is both safe and biocompatible in mammalian cancer conditions.

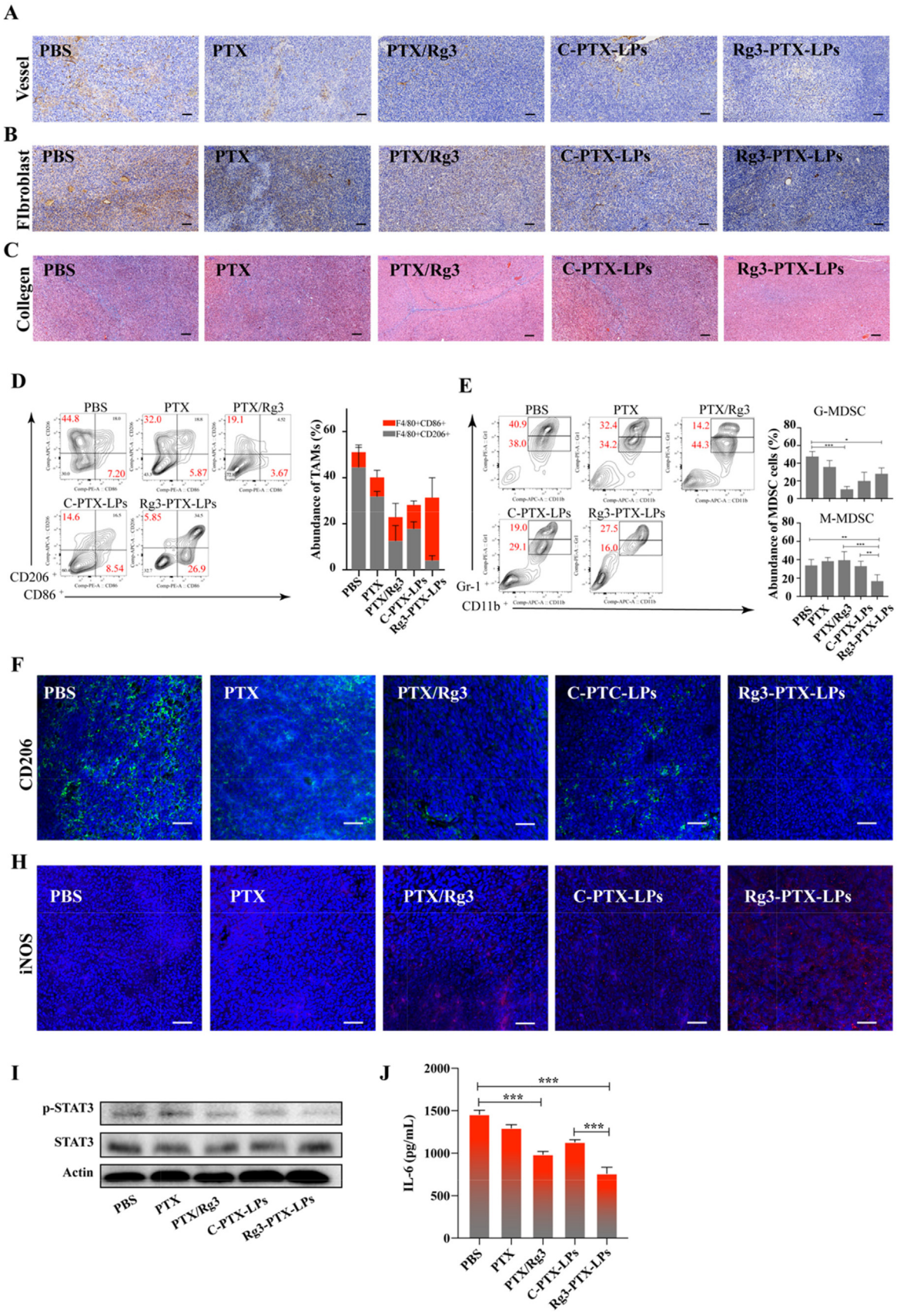
A
Vessel
PBS
PTX
PTX/Rg3
C-PTX-LPs
Rg3-PTX-LPs
B
Fibroblast
C
Collegen
D
CD206+
CD86+
Abundance of TAMs (%)
F4/80+CD86+
F4/80+CD206+
E
Gr-1+
CD11b+
G-MDSC
M-MDSC
Abundance of MDSC cells (%)
F
CD206
C-PTC-LPs
H
iNOS
I
p-STAT3
STAT3
Actin
J
IL-6 (pg/mL)

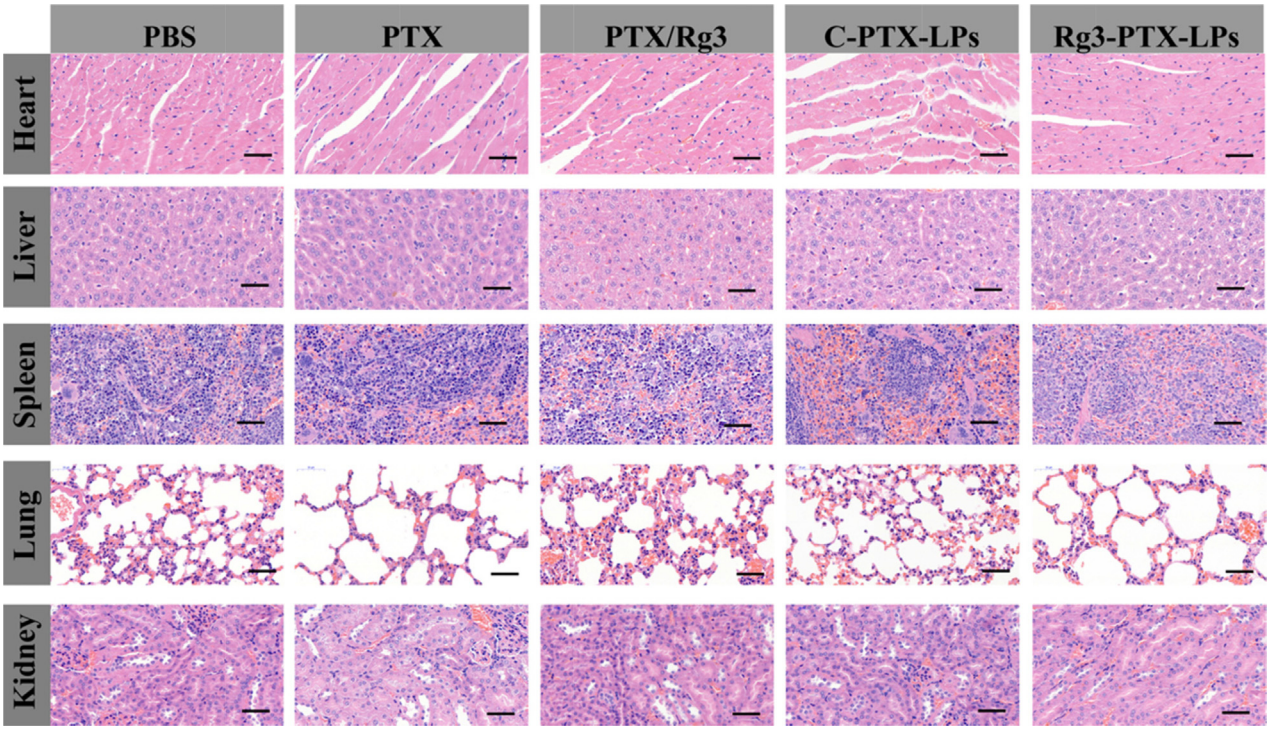

Fig. 9. Histopathological examination of major organs collected from nude mice bearing MCF-7/T cells subcutaneous xenograft tumors after the indicated treatments. Scale bar 50 μm.

Conclusions

We prepared PTX-loaded functional ginsenoside Rg3 liposomes for the treatment of breast tumors. This delivery system can target MCF-7/T tumor cells by interacting with GLUT-1. The combination of PTX and Rg3 was highly efficient in inhibiting MCF-7/T cell proliferation. Therapeutic mechanisms involved enhancing apoptosis, downregulating P-gp and PD-L1, inhibiting angiogenesis, and reeducating the TAM; thus, remodeling the TME by inhibiting IL-6/STAT3/p-STAT3 pathway activation. The Rg3-PTX-LPs delivery system targets the drug into the tumor, reverses cancer drug resistance, and significantly amplifies the antitumor effect. This treatment system represents a potential strategy for anti-MDR cancer therapy programs.

CRediT authorship contribution statement

Ying zhu: Conceptualization, Data curation, Formal analysis, Methodology, Project Administration, Writing – original draf, Writing – review and editing. **Anni Wang and Shuya Zhang:** Methodology, Software. **Jisu KIm, Jiaxuan Xia, Fengxue Zhang and Dan Wang:** Software, Visualization. **Qi Wang and Jianxin Wang:** Resource, Supervision, Validation, Funding acquisition, Writing – review and editing.

Funding

The National Natural Science Foundation of China (award numbers 81773911, 81690263, and 81573616) and the Shanghai Peak Disciplines-Integrated Medicine Development Project supported this research (grant no. 20180101).

Compliance with ethics requirements

All Institutional and National Guidelines for the care and use of animals (fisheries) were followed.

All experiments involving animals were conducted according to the ethical policies and procedures approved by the ethics committee of the Fudan University, Shanghai, China (Approval no. SYXK 2020–0032).

Declaration of Competing Interest

The authors declare that they have no known competing financial interests or personal relationships that could have appeared to influence the work reported in this paper.

Fig. 8. Rg3-PTX-LPs remodel the TME structure of MCF-7/T tumors in an *in vivo* mice model. (A) At the end of the study, vessels in MCF-7/T tumors were processed for immunohistochemical staining of CD31. (B) At the end of the study, TAFs in MCF-7/T tumor tissues were processed for immunohistochemical staining for α-SMA. (C) At the end of the study, collagen fibers in MCF-7/T tumor tissues were stained with Masson's trichrome. (Masson's trichrome stains muscle red and collagen blue) (D) Percentages of TAM populations with specific macrophage markers (M1-type, $CD11b^+/F4/80^+/CD86^+$, and M2-type, $CD11b^+/F4/80^+/CD206^+$) in tumor tissues, as detected by flow cytometry. (E) Flow-cytometry gating and quantitative analysis of $CD11b^+/Gr\text{-}1^+$ MDSCs in tumors. Double-positive cells comprise two populations, including $Gr\text{-}1^{high}CD11b^+$ granulocytic (G-MDSCs) and $Gr\text{-}1^{int}CD11b^+$ monocytic (M−MDSCs) MDSC subsets. (F) CD206 expression (M2 macrophages) in MCF-7/T tumors tissues assessed by confocal microscopy. (H) iNOS expression (M1 macrophages) in MCF-7/T tumors tissues assessed by confocal microscopy. (I) Western blotting of STAT3 and p-STAT3 expression in tumor tissues after treatments. (J) Tumor IL-6 levels after treatments assessed by ELISA. Data are mean ± SD, n = 3, $^*p < 0.05$, $^{**}p < 0.01$, $^{***}p < 0.001$.

Acknowledgements

We also thank Dr. Dan Wang at Xiamen Ginposome Pharmatech Co., Ltd for offering with Rg3 compound.

Appendix A. Supplementary data

Supplementary data to this article can be found online at https://doi.org/10.1016/j.jare.2022.09.007.

References

[1] Sun Y-S, Zhao Z, Yang Z-N, Xu F, Lu H-J, Zhu Z-Y, et al. Risk factors and preventions of breast cancer. Int J Biol Sci 2017;13(11):1387–97.
[2] Rutqvist LE, Cedermark B, Glas U, Johansson H, Rotstein S, Skoog L, et al. Radiotherapy, chemotherapy, and tamoxifen as adjuncts to surgery in early breast cancer: a summary of three randomized trials. Int J Radiat Oncol Biol Phys 1989;16(3):629–39.
[3] Foo J, Michor F. Evolution of acquired resistance to anti-cancer therapy. J Theor Biol 2014;355:10–20.
[4] Huang Y, Li Y. Drug Delivery and Reversal of MDR. Mol Pharm 2014;11 (8):2493–4.
[5] Ling V. Multidrug resistance: molecular mechanisms and clinical relevance. Cancer Chemother Pharmacol 1997;40(7):S3–8.
[6] Zhang P, Ma Y, Lv C, Huang M, Li M, Dong B, et al. Upregulation of programmed cell death ligand 1 promotes resistance response in non-small-cell lung cancer patients treated with neo-adjuvant chemotherapy. Cancer Sci 2016;107 (11):1563–71.
[7] Chen J, Jiang CC, Jin L, Zhang XD. Regulation of PD-L1: a novel role of pro-survival signalling in cancer. Ann Oncol : Off J Eur Soc Med Oncol 2016;27 (3):409–16.
[8] Yaghoubi N, Soltani A, Ghazvini K, Hassanian SM, Hashemy SI. PD-1/ PD-L1 blockade as a novel treatment for colorectal cancer. Biomed Pharmacother 2019;110:312–8.
[9] Fujita Yu, Yagishita S, Hagiwara K, Yoshioka Y, Kosaka N, Takeshita F, et al. The Clinical Relevance of the miR-197/CKS1B/STAT3-mediated PD-L1 Network in Chemoresistant Non-small-cell. Lung Cancer 2015;23(4):717–27.
[10] Balkwill FR, Capasso M, Hagemann T. The tumor microenvironment at a glance. J Cell Sci 2012;125:5591–6.
[11] Chanmee T, Ontong P, Konno K, Itano N. Tumor-associated macrophages as major players in the tumor microenvironment. Cancers 2014;6(3):1670–90.
[12] Yin Y, Yao S, Hu Y, Feng Y, Li M, Bian Z, et al. The immune-microenvironment confers chemoresistance of colorectal cancer through macrophage-derived IL6. Clin Cancer Res; 2017; 23: 7375-87.
[13] Zhu X, Shen H, Yin X, Long L, Chen X, Feng F, et al. IL-6R/STAT3/miR-204 feedback loop contributes to cisplatin resistance of epithelial ovarian cancer cells. Oncotarget 2017;8(24):39154–66.
[14] Dudley AC. Tumor endothelial cells. Cold Spring Harb Perspect Med 2012; 2: 1-18.
[15] Li Y-J, Lei Y-H, Yao N, Wang C-R, Hu N, Ye W-C, et al. Autophagy and multidrug resistance in cancer. Chin J Cancer 2017;36(1). doi: https://doi.org/10.1186/s40880-017-0219-2.
[16] Saraswathy M, Gong S. Different strategies to overcome multidrug resistance in cancer. Biotechnol Adv 2013;31(8):1397–407.
[17] Hu C-M, Zhang L. Nanoparticle-based combination therapy toward overcoming drug resistance in cancer. Biochem Pharmacol 2012;83 (8):1104–11.
[18] Ma L, Kohli M, Smith A. Nanoparticles for combination drug therapy. ACS Nano 2013;7(11):9518–25.
[19] Batist G, Gelmon KA, Chi KN, Miller WH, Jr., Chia SK, Mayer LD, *et al.* Safety, pharmacokinetics, and efficacy of CPX-1 liposome injection in patients with advanced solid tumors. Clin Cancer Res 2009; 15: 692-700.
[20] Wang J-H, Nao J-F, Zhang M, He P. 20(s)-ginsenoside Rg3 promotes apoptosis in human ovarian cancer HO-8910 cells through PI3K/Akt and XIAP pathways. Tumor Biol 2014;35(12):11985–94.
[21] Choi YJ, Lee HJ, Kang DW, Han IH, Choi BK, Cho WH. Ginsenoside Rg3 induces apoptosis in the U87MG human glioblastoma cell line through the MEK signaling pathway and reactive oxygen species. Oncol Rep 2013;30:1362–70.
[22] Mochizuki M, Yoo YungChoon, Matsuzawa K, Sato K, Saiki I, Tonooka S, et al. Inhibitory effect of tumor metastasis in mice by saponins, ginsenoside-Rb2, 20 (R)- and 20(S)-ginsenoside-Rg3, of red ginseng. Biol Pharm Bull 1995;18 (9):1197–202.
[23] Shan X, Fu YS, Aziz F, Wang XQ, Yan Q, Liu JW. Ginsenoside Rg3 inhibits melanoma cell proliferation through down-regulation of histone deacetylase 3 (HDAC3) and increase of p53 acetylation. PLoS One 2014; 9: e115401.
[24] Yue PYK, Wong DYL, Wu PK, Leung PY, Mak NK, Yeung HW, et al. The angiosuppressive effects of 20(R)- ginsenoside Rg. Biochem Pharmacol 2006;72:437–45.
[25] Sato K, Mochizuki M, Saiki I, Yoo YungChoon, Samukawa K, Azuma I. Inhibition of tumor angiogenesis and metastasis by a saponin of Panax ginseng, ginsenoside-Rb2. Biological Pharmaceutical Bulletin 1994;17(5):635–9.
[26] Liu C, Gong Q, Chen T, Lv J, Feng Z, Liu P, et al. Treatment with 20(S)-ginsenoside Rg3 reverses multidrug resistance in A549/DDP xenograft tumors. Oncol Lett 2018;15:4376–82.
[27] Kwon H-Y, Kim E-H, Kim S-W, Kim S-N, Park J-D, Rhee D-K. Selective toxicity of ginsenoside Rg3 on multidrug resistant cells by membrane fluidity modulation. Arch Pharm Res 2008;31(2):171–7.
[28] Chen Z, Wei X, Shen L, Zhu H, Zheng X. 20(S)-ginsenoside-Rg3 reverses temozolomide resistance and restrains epithelial-mesenchymal transition progression in glioblastoma. Cancer Sci 2019;110(1):389–400.
[29] Kim SW, Kwon HY, Chi DW, Shim JH, Park JD, Lee YH, et al. Reversal of P-glycoprotein-mediated multidrug resistance by ginsenoside Rg. Biochem Pharmacol 2003;65:75–82.
[30] Jiang Z, Yang Y, Yang Y, Zhang Yu, Yue Z, Pan Z, et al. Ginsenoside Rg3 attenuates cisplatin resistance in lung cancer by downregulating PD-L1 and resuming immune. Biomed Pharmacother 2017;96:378–83.
[31] Kang S, Park S-J, Lee A-Y, Huang J, Chung H-Y, Im D-S. Ginsenoside Rg3promotes inflammation resolution through M2 macrophage polarization. J Ginseng Res 2018;42(1):68–74.
[32] Shao M, Qiu J, Wu H, Liu Y, Liu L. Mechanism of Shenyi Capsule concomitant with endostar and chemotherapy on the growth and apoptosis of MCF-7 breast cancer cells. J Int Translat Med 2014;2:299–302.
[33] Jiwei L, Liangxin S, Yi Z, al e. Clinical Phase II Study on Immunoimprovement of Patients with Breast Cancer Treated by Shenyi Capsule. Chin J Clin Oncol 2000; 27: 534-6.
[34] Huang JY, Sun Y, Fan QX. Efficacy of Shenyi Capsule combined with gemcitabine plus cisplatin in treatment of advanced esophageal cancer:a randomized controlled trial. J Chin Integrat Med 2009;7:1047.
[35] Ranney DF. Biomimetic transport and rational drug delivery. Biochem Pharmacol 2000;59(2):105–14.
[36] Ying X, Wen He, Lu W-L, Du Ju, Guo J, Tian W, et al. Dual-targeting daunorubicin liposomes improve the therapeutic efficacy of brain glioma in animals. J Controlled Release Off J Controlled Release Soc 2010;141(2):183–92.
[37] Brown RS, Wahl RL. Overexpression of Glut-1 glucose transporter in human breast cancer. An immunohistochemical study. Cancer 1993;72(10):2979–85.
[38] Zhao FQ, Keating AF. Functional properties and genomics of glucose transporters. Curr Genomics 2007;8:113–28.
[39] Takata K, Kasahara T, Kasahara M, Ezaki O, Hirano H. Erythrocyte/HepG2-type glucose transporter is concentrated in cells of blood-tissue barriers. Biochem Biophys Res Commun 1990;173(1):67–73.
[40] Joost H-G, Thorens B. The extended GLUT-family of sugar/polyol transport facilitators: nomenclature, sequence characteristics, and potential function of its novel members. Mol Membr Biol 2001;18(4):247–56.
[41] Pardridge WM. Vector-mediated peptide drug delivery to the brain. Adv Drug Deliv Rev 1995;15(1-3):109–46.
[42] Hong C, Wang D, Liang J, Guo Y, Zhu Y, Xia J, et al. Novel ginsenoside-based multifunctional liposomal delivery system for combination therapy of gastric cancer. Theranostics 2019;9(15):4437–49.
[43] Zhu Y, Liang J, Gao C, Wang A, Xia J, Hong C, et al. Multifunctional ginsenoside Rg3-based liposomes for glioma targeting therapy. J Control Release 2021;330:641–57.
[44] Hong SS, Choi JY, Kim JO, Lee MK, Kim SH, Lim SJ. Development of paclitaxel-loaded liposomal nanocarrier stabilized by triglyceride incorporation. Int J Nanomed 2016;11:4465–77.
[45] Modi S, Anderson BD. Determination of drug release kinetics from nanoparticles: overcoming pitfalls of the dynamic dialysis method. Mol Pharm 2013;10(8):3076–89.
[46] The isolation and characterization of murine macrophages. Current Protocols in Immunology 2015;83:11–4.
[47] Levi J, Cheng Z, Gheysens O, Patel M, Chan CT, Wang Y, et al. Fluorescent fructose derivatives for imaging breast cancer cells. Bioconjug Chem 2007;18 (3):628–34.
[48] Pardridge WM. Preface: Overview of brain drug delivery. Adv Drug Deliv Rev 1995;15(1-3):1–3.
[49] Koopman G, Reutelingsperger CP, Kuijten GA, Keehnen RM, Pals ST, van Oers MH. Van Annexin V for flow cytometric detection of phosphatidylserine expression on B cells undergoing apoptosis. Blood 1994;84(5):1415–20.
[50] Gao CZ, Yang PM, Yan LG. Studies of 20(R)-ginsenoside Rg3 on reversal multidrug resistance (MDR) and induction of apoptosis in K562/ADM cell line. Progr Anatomical Sci 2002;8:31–5.
[51] Mantovani A, Sozzani S, Locati M, Allavena P, Sica A. Macrophage polarization: tumor-associated macrophages as a paradigm for polarized M2 mononuclear phagocytes. Trends Immunol 2002;23(11):549–55.
[52] Javeed A, Ashraf M, Riaz A, Ghafoor A, Afzal S, Mukhtar MM. Paclitaxel and immune system. Eur J Pharm 2009;38(4):283–90.
[53] Lee JW, Choi YR, Mok HJ, Seong H-A, Lee DY, Kim G-S, et al. Characterization of the changes in eicosanoid profiles of activated macrophages treated with 20 (S)-ginsenoside Rg3. J Chromatogr B Analyt Technol Biomed Life 2017;1065-1066:14–9.
[54] Majidinia M, Yousefi B. Breast tumor stroma: A driving force in the development of resistance to therapies. Chem Biol Drug Des 2017;89 (3):309–18.
[55] Castells M, Thibault B, Delord J-P, Couderc B. Implication of tumor microenvironment in chemoresistance: tumor-associated stromal cells protect tumor cells from cell death. Int J Mol Sci 2012;13(8):9545–71.
[56] Brown Y, Hua S, Tanwar PS. Extracellular matrix-mediated regulation of cancer stem cells and chemoresistance. Int J Biochem Cell Biol 2019;109:90–104.

[57] Senthebane DA, Rowe A, Thomford NE, Shipanga H, Munro D, Mazeedi MAMA, et al. The role of tumor microenvironment in chemoresistance: to survive, keep your enemies closer. Int J Mol Sci 2017;18(7):1586. doi: https://doi.org/10.3390/ijms18071586.
[58] Chen Y, Yu Q, Xu CB. A convenient method for quantifying collagen fibers in atherosclerotic lesions by ImageJ software. Int J Clin Exp Med 2017;10:14904–10.
[59] Lee SH, Starkey PM, Gordon S. Quantitative analysis of total macrophage content in adult mouse tissues. Immunochemical studies with monoclonal antibody F4/80. J Exp Med 1985;161:475–89.
[60] Chávez Galán L, Olleros ML, Vesin D, Garcia I. Much more than M1 and M2 macrophages, there are also CD169(+) and TCR(+) macrophages. Front Immunol 2015;6:263–4.
[61] Gabrilovich DI, Nagaraj S. Myeloid-derived suppressor cells as regulators of the immune system. Nat Rev Immunol 2009;9(3):162–74.
[62] Yu H, Kortylewski M, Pardoll D. Crosstalk between cancer and immune cells: role of STAT3 in the tumour microenvironment. Nat Rev Immunol 2007;7(1):41–51.
[63] Zhao C, Li H, Lin H-J, Yang S, Lin J, Liang G. Feedback activation of STAT3 as a cancer drug-resistance mechanism. Trends Pharmacol Sci 2016;37(1):47–61.
[64] Poh AR, Ernst M. Targeting macrophages in cancer: from bench to bedside. Front Oncol 2018;8:49–50.
[65] Wang SW, Sun YM. The IL-6/JAK/STAT3 pathway: potential therapeutic strategies in treating colorectal cancer. Int J Oncol 2014;44:1032–40.
[66] Teng Y-N, Kao M-C, Huang S-Y, et al. Novel application of rhein and its prodrug diacerein for reversing cancer-related multidrug resistance through the dual inhibition of P-glycoprotein efflux and STAT3-mediated P-glycoprotein expression[J]. Biomed Pharmacother 2022;150:112995.